Research article

Fabio Gabelloni, Francesco Biccari, Naomi Falsini, Nicola Calisi, Stefano Caporali
and Anna Vinattieri*

Long-living nonlinear behavior in CsPbBr$_3$ carrier recombination dynamics

Abstract: By means of time-resolved photoluminescence
(TR-PL) spectroscopy, we present a detailed investigation
of the carrier relaxation dynamics in a CsPbBr$_3$ bulk sam-
ple and microcrystal ensemble at cryogenic temperature
on a picosecond time scale. We provide evidence of a long
temperature-dependent cooling rate for the excitons and
free carriers population, with an initial cooling time con-
stant of a few tens of picoseconds. A relaxation bottleneck
in the thermalization process was found that cannot be
explained by the Auger effect or hot phonon population,
since we address a very low excitation regime, not com-
monly investigated in literature, where such processes
are not effective. Adding a continuous wave optical bias
to the picosecond excitation, we probed the photoinduced
PL decrease of the localized states and the photoinduced
PL increase of the population in the high energy states.
A long recovery time from the photoinduced PL decrease
was found for localized states and quite significant dif-
ferences were detected, depending on the resonance/off
resonance bias used in the experiment.

Keywords: inorganic perovskites; CsPbBr$_3$; time-
resolved optical spectroscopy; excitons; thermalization;
non-linearity.

*Corresponding author: Anna Vinattieri, Dipartimento di Fisica e
Astronomia, Università di Firenze, via G.Sansone 1, 50019 Sesto
Fiorentino, Italy; LENS, via N.Carrara 1, 50019 Sesto Fiorentino, Italy;
and INFN, Sezione Firenze, via G.Sansone 1, 50019 Sesto Fiorentino,
Italy, e-mail: vinattieri@fi.infn.it. https://orcid.org/0000-0002-
0781-4002
Fabio Gabelloni and Naomi Falsini: Dipartimento di Fisica e
Astronomia, Università di Firenze, via G.Sansone 1, 50019 Sesto
Fiorentino, Italy
Francesco Biccari: Dipartimento di Fisica e Astronomia, Università
di Firenze, via G.Sansone 1, 50019 Sesto Fiorentino, Italy; and LENS,
via N.Carrara 1, 50019 Sesto Fiorentino, Italy
Nicola Calisi and Stefano Caporali: Dipartimento di Ingegneria
Industriale, Università di Firenze, via Santa Marta 3, 50139 Firenze, Italy

1 Introduction

Perovskites (PVK), hybrid organic-inorganic (H-PVK) and
fully inorganic (I-PVK), are innovative materials with
extreme relevance with regards to applications that span
from photovoltaics [1–3] to LED, lasers [4–7], sensors [8, 9]
and generally speaking, optoelectronic devices, given their
peculiar characteristics. In fact the low-cost chemical syn-
thesis, the band-gap tunability, which is easily controlled
by the composition, the possibility of several types of nano-
structures, etc. [10] make PVK a possible substitute of III–V
and IV semiconductors for innovative devices. The huge
experimental and theoretical numbers of studies in the
last decade confirm the interest of the scientific commu-
nity in such materials. Most of the research has focused on
H-PVK, especially as active materials for photovoltaic cells.
However, several technological issues limit the perfor-
mances of H-PVK, such as chemical instability, especially
in the presence of moisture and after UV light exposure,
and thermal instability, all effects that produce degrada-
tion and decomposition of the material [11–13]. Removing
the organic part, which is mainly responsible for H-PVK
degradation, has proved successful. Therefore, after the
seminal work of Protesescu et al. [14], a great part of the
research activity in this field was directed to I-PVK, in par-
ticular CsPbX$_3$ (X = Cl, Br, I), as I-PVK are more suitable for
applications where a long lifetime of the device is manda-
tory. As typical of research devoted to the development of
new materials for innovative optoelectronic devices, a deep
knowledge of the processes that rule the recombination
dynamics of the carriers and excitons, and the relationship
with the material crystallinity and stoichiometry, is nec-
essary. In the case of PVK, since most of the investigated
samples are assembled in the form of nanoparticles or
microcrystals, it is clear that surface states can play a major
role, affecting both the optical and electrical properties.
For some applications recently under investigation such as
high energy particle detectors [15, 16], bulk crystals (single
or polycrystalline) are of interest; in this case, other kinds
of defects, such as shallow or deep traps, can affect the

recombination. Therefore, a comparative study of a bulk and a microcrystalline sample is relevant when considering that a different morphology/size is required depending on the specific application intended for the material.

Up to now, most studies concerning the recombination dynamics in I-PVK have addressed the room temperature regime, which is of course relevant for device operation. However, in order to gain a deep knowledge of the processes influencing the carrier recombination, it is also necessary to investigate the low temperature regime. In this paper, we present time-resolved photoluminescence (TR-PL) spectra of different CsPbBr₃ samples (bulk sample [CR] and spin-coated [SC] microcrystal ensemble) to study the relaxation dynamics of free carriers and excitons in a low excitation regime (excitation density $\delta \approx 10^{16}/cm^3$ carriers per pulse). In particular, we focus on the carrier thermalization regime that, on a picosecond time scale, is dominated by the interaction of the carriers with acoustic phonons. By adding a nonresonant/resonant continuous wave (CW) bias to the nonresonant excitation pulse, we show the significant nonlinearity in the recombination dynamics for the low energy/high energy states of the PL band.

2 Experimental

Two different CsPbBr₃ samples were investigated: a bulk sample (CR) and a SC microcrystal ensemble deposited on a glass substrate. In both cases, a CsPbBr₃ solution was prepared by dissolving equal molar quantities of the precursors (CsBr and PbBr₂) in dimethyl sulfoxide. The solution was stirred overnight to obtain a clear liquid. For the microcrystal ensemble, after the spinning, the sample was dried and annealed at 393 K for 10 min. The CsPbBr₃ bulk sample was grown by antisolvent vapor-assisted crystallization (AVC) method [17], using methanol as antisolvent. Samples were finally encapsulated in a poly(methyl methacrylate) (PMMA) layer.

Scanning electron microscopy images of the bulk sample and of the SC sample are shown in Figure 1. It is worth noting the large size of CR, which was of the order of 1 mm, and its flat surfaces, indicating a very good optical quality. The X-ray diffraction (XRD) pattern reported in Figure 1C shows the presence of a few differently oriented crystalline domains, by the splitting of the diffraction spots, as shown in the inset. Evidence of a polycrystalline structure is commonly reported (e.g. ref. [18]) and the origin of the diffraction spots can be ascribed to twinning phenomena [15]. The SC sample consists of a collection of microcrystals, well separated among each other, with a large spread in size, from hundreds of nanometers to several micrometers. XRD analysis at room temperature indicates
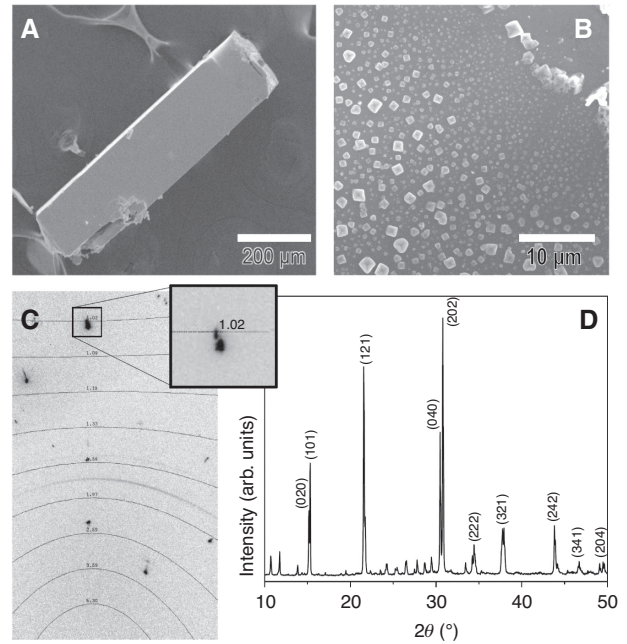
Figure 1: Morphological and structural characterization of the samples. Scanning electron microscopy (SEM) images of the bulk sample (A) and the spin-coated microcrystalline film (B) and their X-ray diffraction (XRD) patterns (C) and (D), respectively. In the case of the bulk sample, the presence of a few differently oriented crystalline domains is evidenced by the splitting of the diffraction spots, as shown in the inset of panel (C). The numbers in (C) correspond to interplanar distances (Å).

only small traces of spurious phases (CsBr and PbBr₂), as shown by the presence of non-indexed peaks in Figure 1D, while the CsPbBr₃ orthorhombic phase dominates.

Low temperature PL experiments were performed in a quasi-backscattering geometry, keeping the samples in a closed cycle cryostat at 10 K. A frequency-doubled mode-locked picosecond Ti-sapphire laser, operating at an 81.3 MHz repetition rate with 1.2 ps long pulses, was used for the TR-PL experiments. The maximum excitation intensity was about 10 W/cm², corresponding to an estimated excitation density δ of about 2×10^{16} cm⁻³ carriers per pulse. TR-PL measurements were carried out using a synchroscan streak camera (time resolution 5 ps) after spectral dispersion of the detected signal through a 25 cm monochromator, equipped with a 300 grooves/mm grating (blaze 500 nm, spectral resolution of 2 meV). Eventually, CW-laser diodes at different wavelengths were used in combination with the picosecond pulses for probing the nonlinear response of the samples.

3 Thermalization of the free carrier population

TR-PL spectroscopy is a very efficient tool to investigate the processes ruling the relaxation and recombination of

carriers and excitons. In this work, firstly we discuss the topic of carrier thermalization.

In Figure 2A, a streak image of the PL time evolution for the bulk sample is shown for the fastest time scale, after nonresonant excitation at 3.35 eV, at a temperature of 10 K. The strong emission at 2.32 eV, which dominates at early times, comes from the free exciton (FE) recombination, as measured from reflectivity (Figure 2D) and in agreement with literature data [15, 18], while the low energy emission below 2.3 eV corresponds to bound exciton (BE) recombination, usually assigned to Br vacancy centers [19].

The Stokes shift value between the PL and the reflectivity spectrum, which resulted in about 2 meV (Figure 2D), is in agreement with literature data [18] and provides evidence of a small inhomogeneous broadening due to disorder.

A significant emission above the FE transition was also detected: from the Arrhenius plot of the PL intensity versus temperature (not shown), we estimate an exciton binding energy of ≈30–35 meV, in agreement with literature data [20]. Therefore, the observation of PL emission at energies above the exciton line has to be ascribed to free carrier recombination (FCR). We want to remark that the polycrystalline nature does not affect the experimental results discussed here and only accounts for the inhomogeneous broadening of the PL spectrum.

PL decays, acquired with the streak camera in a time interval up to 800 ps, are shown in Figure 2B: non-exponential decays are shown at the BE and FE energies, while the FCR decay turns out to be exponential with a decay time of ≈50 ps. An estimate of the initial time decay constant gives values of about 80 and 120 ps for the FE and

BE emissions, respectively. Figure 2C shows the risetime of the PL at the same energies as Figure 2B: for the FCR, the risetime is ≈10 ps, while it is ≈20 ps (30 ps) for FE (BE). The time-integrated spectrum is shown for the same experimental conditions in Figure 2D. The PL decay times measured for the different emissions (BE, FE, FCR) agree with literature data at low temperatures [21, 22]. The fast decay of FCR cannot be ascribed to surface recombination as indicated in ref. [23], because in consideration of the absorption length (≈100 nm) in our experimental conditions, it would require a very high mobility, not found in CsPbBr$_3$ [24, 25]. Instead it is mainly due to the exciton formation, as also confirmed by its slightly superlinear dependence on the excitation power that is evidence of a prevalence of the exciton formation with respect to the other FCR decay channels.

From the streak images, such as the one shown in Figure 2, we can extract TR spectra at different delays; a set of spectra are shown in Figure 3.

From Figures 2C and 3A, it can clearly be seen that the FE emission rises in about 15–20 ps, with a delay of 5–10 ps with respect to the FCR. This corresponds to the transfer of the FE from the high energy non radiative states into the $K \leq K_{ph}$ radiative states, where K and K_{ph} indicate the exciton and photon wavevectors, respectively [26]. Given the rise time and the carrier density value we can infer for the bimolecular exciton formation coefficient (C) at 10 K a lower limit $C = 5 \times 10^{-6}$ cm^3 s^{-1}, to be compared, for example with that of GaN where $C = 1.2 \times 10^{-6}$ cm^3 s^{-1} [27]. The emission from FE initially dominates the PL spectra, and successively the excitons localize in shallow states and form bound excitons; Moreover a long living Urbach tail is
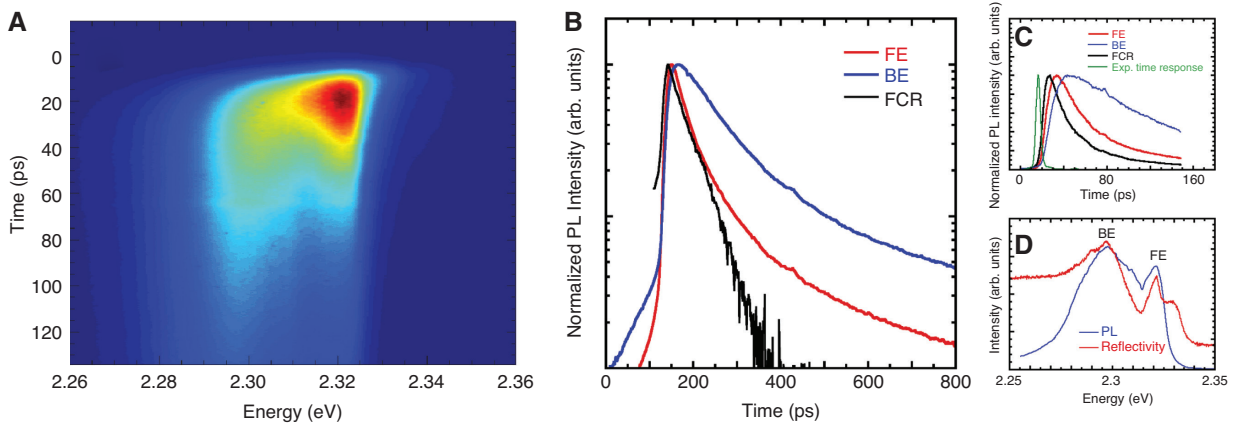
Figure 2: Bulk sample.
(A) Photoluminescence (PL) time evolution after picosecond excitation at 3.35 eV. (B) PL decay at free carrier recombination (FCR), free exciton (FE) and bound exciton (BE) energies (log scale). (C) Rise of the PL for the FCR, FE and BE energies (linear scale). In green, the experimental time response is reported. (D) Time-integrated PL spectrum (blue) compared with the reflectivity spectrum (red). All the measurements reported in the figures were performed at 10 K.
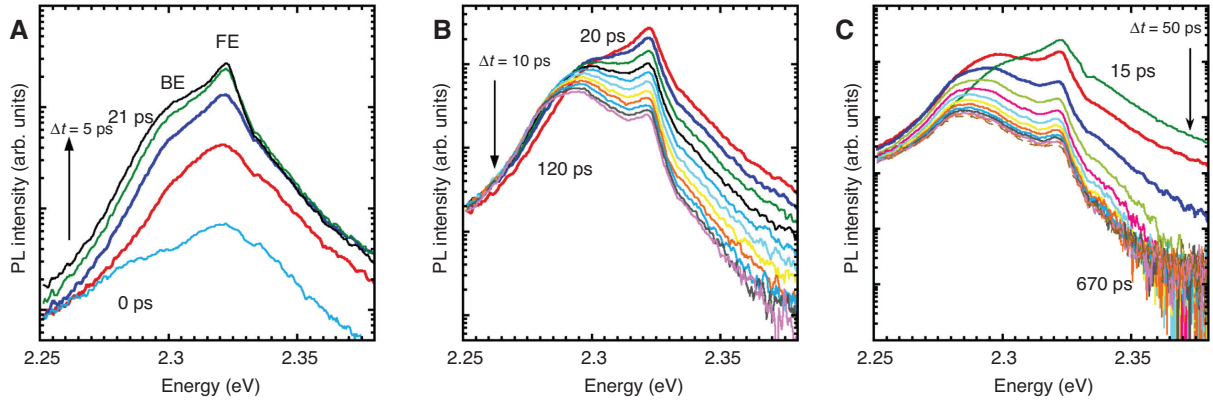
Figure 3: Bulk sample.
Time-resolved photoluminescence (TR-PL) spectra (in log scale) as extracted from streak images in different time scales. For each spectrum, the time delay with respect to the excitation is reported, while Δt corresponds to the time interval between two adjacent spectra. (A) Rise of the TR-PL, (B) early decay times, (C) longer decay times.

detected, arising from localized states. A faster rise and decay is observed for the PL signal detected in the high energy side above the FE emission where the contribution comes from the free carriers recombination. From the TR spectra of Figure 3, it is seen that the high energy side of the PL, above the FE state, is characterized by an exponential tail with a slope which becomes steeper, increasing the delay. The presence of the exponential tail is evidence of a thermalization condition for the carriers, where the population can be described, in the non-degenerate case, by a Boltzmann distribution with an effective temperature T_{eff}, which is a function of time [26]. Therefore, we can express the PL intensity I at a given time t by:

$$I(t) \propto \text{DOS}(E) \exp\left(-\frac{E}{K_B T_{eff}(t)}\right) \qquad (1)$$

where DOS(E) indicates the density of states and the effective temperature T_{eff} depends on time. As seen from Figure 3C, after about 0.2 ns, the slope of the high energy tail does not show any remarkable further change, with a very slow decay. From an exponential fit of the high energy tail of the TR-PL spectrum at a time delay of 670 ps where $T_{eff} = T_{fin}$, we find that $T_{fin} = 45$ K. From Eq. (1), we can extract the DOS(E), shown in Figure 4A, where for comparison, a TR-PL spectrum at a time delay of 156 ps is shown. In the DOS(E), the excitonic peak at 2.32 eV clearly comes out.

From Eq. (1), we find an exponential dependence on the energy for the quantity

$$A(t, T) = \frac{I(t, T_{eff})}{I(t_{\infty}, T_{fin})}$$
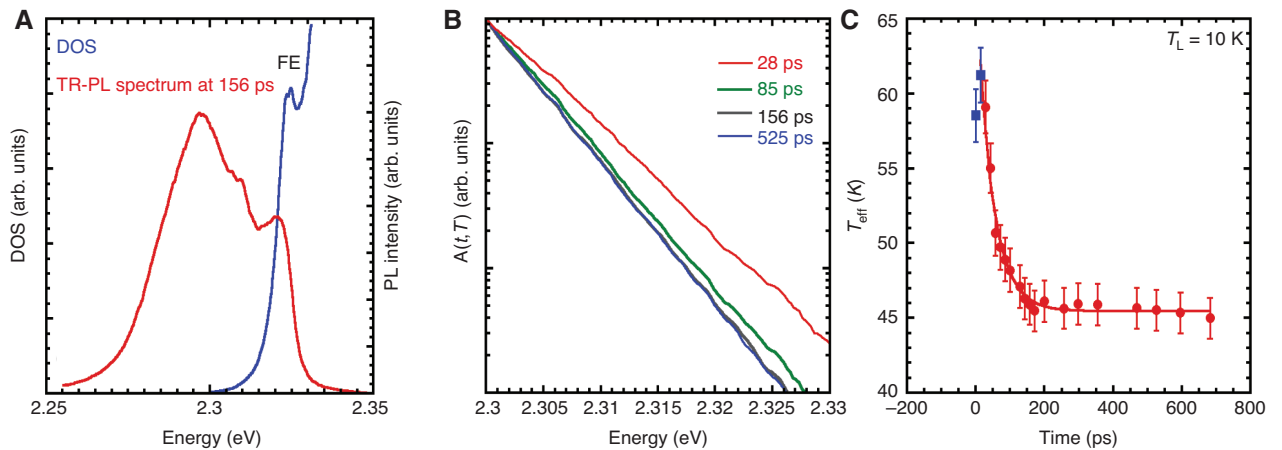
Figure 4: Bulk sample.
(A) Density of states (DOS) extracted from time-resolved photoluminescence (TR-PL) spectra, as discussed in the text, along with a TR-PL spectrum at 10 K. (B) $A(t, T)$ for different time delays (log scale). (C) Effective temperature of the carriers T_{eff} as a function of time delay. The red points refer to a thermal distribution, while the blue ones refer to an incomplete thermalization condition. The solid line in (C) is a fit with Eq. (2).

as illustrated in Figure 4B for a few TR-PL spectra. From such dependence, we can extract T_{eff} which is plotted as a function of the time delay in Figure 4C, for a lattice temperature $T_L = 10$ K. An evident bottleneck in the relaxation is found and the effective temperature remains around 45 K for hundreds of picoseconds, after a fast initial decay. The blue points in Figure 4C correspond to TR-PL spectra (in the rise of the PL signal up to about 20 ps) where we can roughly estimate a temperature, but the thermalization is incomplete. Given the excitation density and the time resolution of our experiments, the thermalization regime that we investigated is dominated by the interaction of the carriers with acoustic phonons. In this case, the time evolution of T_{eff} can be reproduced by [28]:

$$T_{eff}(t) = T_\infty \star \left(\frac{A\exp\left(\dfrac{t}{\tau_1}\right) + 1}{A\exp\left(\dfrac{t}{\tau_1}\right) - 1} \right)^2 \tag{2}$$

corresponding to a temperature (energy) relaxation of the free carriers due to the carrier-acoustic phonon interaction via the deformation potential [29]. In Eq. (2), T_∞ indicates the final temperature (that should be the lattice temperature), τ_1 is the time constant describing the fast relaxation and $A = \dfrac{\sqrt{T_0} + \sqrt{T_\infty}}{\sqrt{T_0} - \sqrt{T_\infty}}$ with T_0 the carrier temperature at $t = 0$. From the fit (solid line in Figure 4C) we get $\tau_1 = 50$ ps, $T_0 = 67$ K and $T_\infty = 45$ K. Such a value for T_∞, higher than the lattice temperature, does not come from a lattice heating, as confirmed by the temperature

dependence of the PL spectra. In fact, at 45 K the bound exciton emission becomes negligible with respect to the free exciton contribution, and by the high energy tail of quasi resonantly excited PL spectra, at 10 K, we extract a carrier temperature lower than 20 K (not shown). As expected from the model discussed in [28, 29], T_∞ should correspond to the lattice value (i.e. 10 K), but TR-PL spectra up to a delay of 1.5 ns show a temperature ($T \approx 30$ K) still above that of the lattice, indicating the presence of a very slow process.

Similar results were also found for the SC microcrystals: in this case, the PL is characterized by a band the peak energy of which, at 10 K, changes between 2.32 eV and 2.39 eV depending on the position on the sample, possibly due to differences in the local strain induced by the substrate [30]. Results for the band at 2.39 eV are shown in Figure 5, along with some normalized TR-PL spectra, extracted from the image of Figure 5, and the effective temperature of the carriers as a function of time delay.

Therefore, also in the case of the SC sample, a significant bottleneck in the temperature relaxation is found with a faster initial decrease of T_{eff} with respect to what is found for the bulk sample. In this case, we get $\tau_1 = 15$ ps, $T_0 = 89$ K and $T_\infty = 58$ K. The results previously shown suggest that the same physical mechanism rules the thermalization both in the bulk and the SC sample. The most relevant difference is the relaxation time, which is three times faster for the SC sample, possibly due to a change of the deformation potential coefficient as a consequence of local strain [29]. To our knowledge, there are no results in the literature concerning this specific topic. With regards to the temperature relaxation at longer time delays, and the slow energy dissipation rate of the FCR, similar
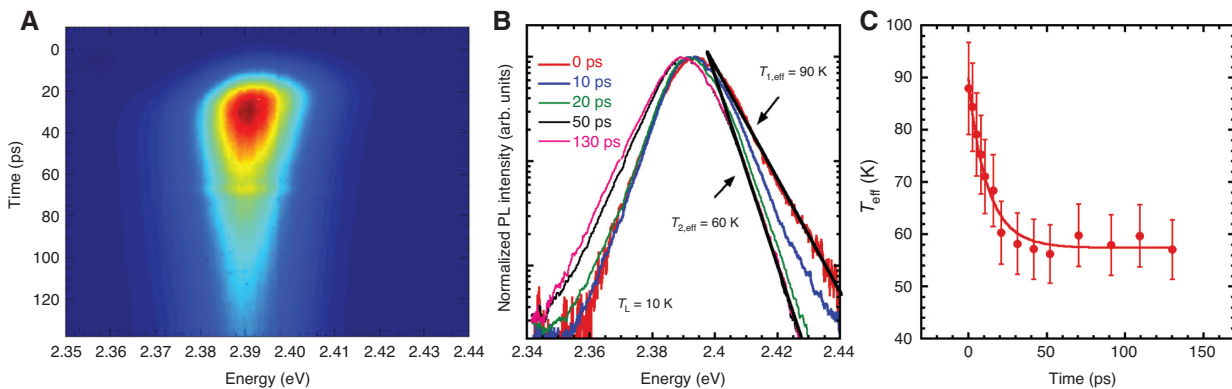
Figure 5: Spin-coated sample.
(A) Streak image. (B) Normalized time-resolved photoluminescence (TR-PL) spectra where the exponential tail is evidenced in black.
(C) Effective temperature of the carriers T_{eff} as a function of time delay: the continuous line is a fit with Eq. (2). Measurements refer to a lattice temperature of 10 K.

behavior is found for both samples, possibly related to a long-living free carrier population, especially in the case of the SC sample.

The relaxation bottleneck in H-PVK and I-PVK nanostructures [31–39] was recently reported and ascribed to several causes such as efficient Auger processes, hot phonons or polaron formations, that keep the carrier temperature higher than the lattice temperature. However, at the excitation density used in our experiment ($\delta \approx 10^{16}$ cm^{-3} carriers per pulse), both hot phonons and Auger heating are negligible, given the Auger coefficient in CsPbBr$_3$ bulk, $3 \times 10^{-27} - 4 \times 10^{-28}$ cm^6 s^{-1} [40]; for the same reason, a screening of the exciton-phonon interaction can be excluded. The large polaron formation has been demonstrated in MAPbBr$_3$ and CsPbBr$_3$ [32, 36] and strongly affects the cooling in the first few picoseconds, but it is not relevant on the time scale we considered in our experiment. Therefore, the origin of the very slow cooling, in a time scale and an energy range where the interaction between free carriers and acoustic phonons prevails, must be searched for outside the previous causes. It is worth remarking that the persistent non negligible FCR population, living several hundreds of picoseconds (e.g. see Figure 2), may be related to the slowing down of the cooling. Persistent energetic electrons have been already observed in MAPbI$_3$ [35] and FAPbI$_3$ [41] and a reduced density of states has recently been proposed as the origin of the slow dynamics and cooling in CsPbI$_3$ [42]. We recently demonstrated [43], for SC samples, that surface states can efficiently trap the carriers, with a long release time, providing a carrier reservoir for the radiative recombination: therefore, surface states can play a role in the thermalization process and similarly in bulk high energy long-living traps eventually related to small structural defects or inclusions (e.g. CsPbBr$_5$, or PbBr$_2$).

4 Nonlinear behavior of excitons and free carriers

TR-PL spectra previously shown reveal the complex nature of the radiative recombination where excitons, both free and bound, and free carriers contribute to the emission. In order to elucidate the interplay between the different populations, we performed TR-PL spectra adding different CW bias to the picosecond excitation pulse [44]. We used a CW laser diode at 405 nm, well above the PL energies for both the bulk and SC samples, a 532 nm laser diode for resonant excitation of the bulk sample and one at 515 nm for resonantly exciting the PL of the SC sample. We aimed to compare the response of the sample in the presence/absence of the bias: in fact, in the case of linear processes the PL, when the bias is added to the picosecond excitation, reproduces the sum of the PL obtained by separate excitation with the bias and the pulse. In some sense, in this way we can provide information similar to a pump-probe experiment and we can test the nonlinearities of the relaxation dynamics and recombination. However, since the maximum power used in our experiment is much lower than the one commonly used in pump-probe experiments, we are able to detect smaller nonlinearities.

In Figure 6A, for the bulk sample, we report the streak image acquired by subtracting the separate contribution to the PL of the CW nonresonant bias (I_b) and of the picosecond excitation (I_p) from the acquisition with both picosecond and bias (I_{pb}). In Figure 6B and C, we show the time evolution of the PL, as extracted from the corresponding streak image (Figure 6A) at different time delays. The low energy side (below 2.31 eV) shows a photoinduced PL decrease (PHD) with a long recovery time. The free exciton at 2.32 eV shows a faster recovery from the PHD with
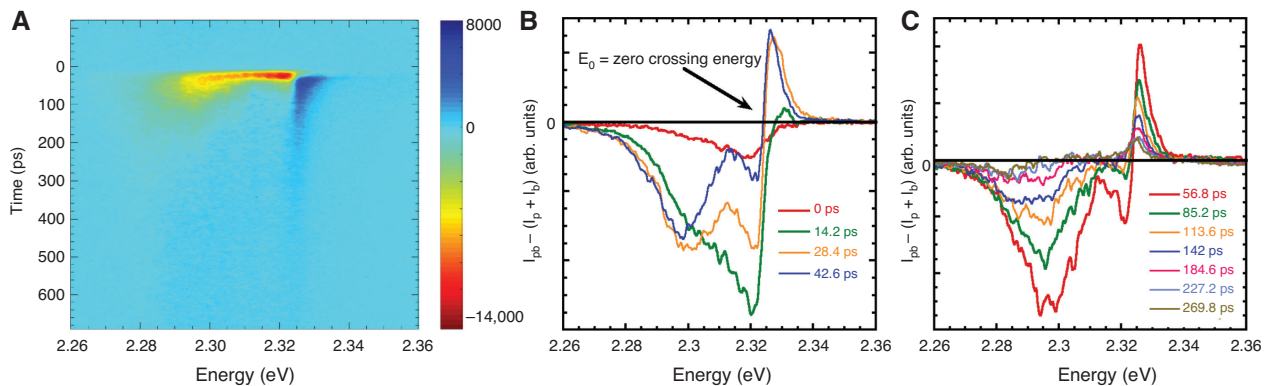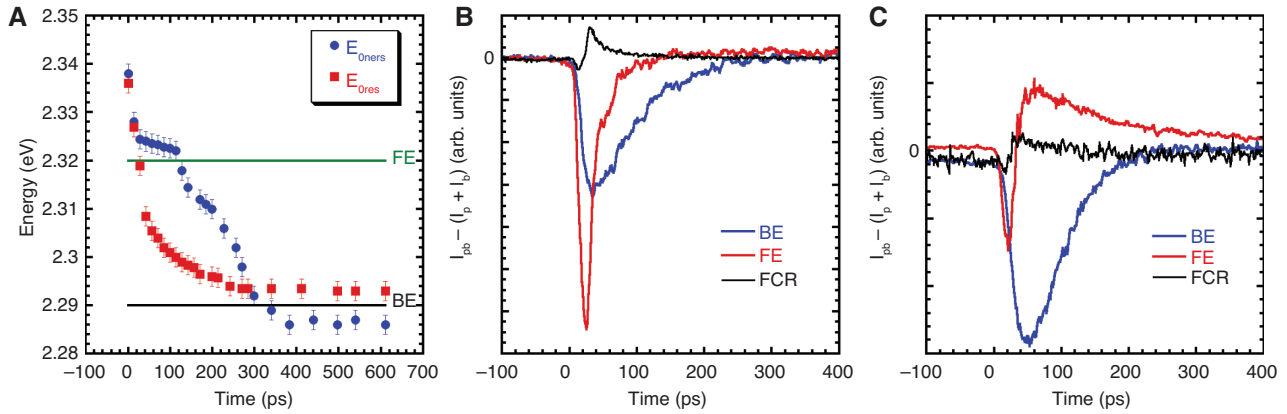

Figure 6: Bulk sample.
(A) Image reporting the time evolution of the nonlinear signal $I_{pb} - (I_p + I_b)$. (B), (C) Time-resolved photoluminescence (TR-PL) spectra extracted from (A).

respect to the bound states, while the free carrier spectral region, after a small initial PHD, shows a photoinduced PL increase (PHI), which can be ascribed to a bimolecular radiative recombination process. It is relevant to note that our experiment allows only the detection of excitons in radiative states and therefore momentum relaxation can require tens of picoseconds, as long as the relaxation process proceeds through low energy phonon emission. In the spectra, the energy E_0 marks the crossover between the sublinear and the superlinear regime.

The results are summarized for the bulk sample in Figure 7, comparing the case of nonresonant and resonant bias, with a power of 500 µW in both cases.

Firstly, as shown in Figure 7A, the significant shift of E_0 with time comes out, corresponding to a relaxation dynamics within the band from the free to the bound states; few hundreds of picoseconds are required before reaching the

complete exciton localization. Quite remarkable, also, is the recovery time from the PHD of the localized emission, again in the time scale of a few hundreds of picoseconds. A PHI is always observed for the FCR emission, as previously stated, because of a bimolecular radiative recombination process. The PHD at the BE energy is a consequence of the partial saturation of the involved sites and persists in time; for the FE the initial PHD can be the result of a partial saturation of the localization sites and/or of a scattering with the free carriers that removes the exciton from the radiative states [44]. In fact, as shown in Figure 7B and C, with the same power of the bias the FE recovery of the superlinear behavior is faster and more pronounced in the resonant case, where a lower density of excitons and FCR is created as a consequence of the lower absorption coefficient. The recovery from the sublinear regime and the transition to a superlinear behavior, coming from the bimolecular exciton

Figure 7: Bulk sample.
(A) Time evolution of the zero-crossing energy E_0. (B), (C) Nonlinear contribution evaluated as indicated in the text for the bulk sample when nonresonant (B) or resonant (C) bias is used for three different spectral regions: the bound exciton (BE), the free exciton (FE), and the free carrier recombination (FCR).
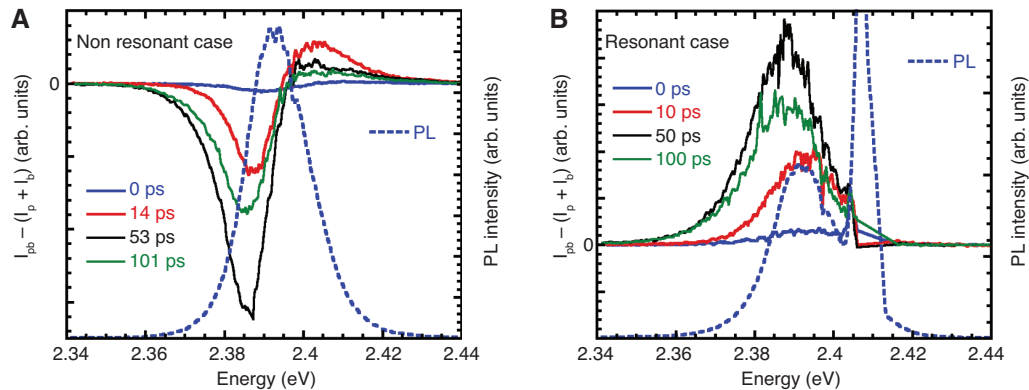
Figure 8: Spin-coated sample.
(A) Nonlinear response for the nonresonant bias. (B) Nonlinear response for the resonant bias. The dashed line (blue) corresponds to the PL signal.

formation process, are faster at the higher energies of the FE band and are evidence of a non negligible contribution related to the localization degree. Results for the SC sample are reported in Figure 8.

The PL spectra of the SC sample do not show a clear signature of the bound exciton band, as observed for the bulk sample, but instead a larger inhomogeneous broadening. The results of Figure 8A indicate a significant photoinduced PL decrease of the low energy side of the emission, with a faster recovery with respect to the bulk sample, which we ascribe mainly to the saturation of the localized sites. The high energy side shows, instead, a photoinduced PL increase due to the free carrier population. Only a superlinear behavior is observed for resonant bias (Figure 8B), because of an efficient exciton formation in our experimental conditions.

We want to emphasize that, even though in our experiment we address only the behavior of excitons and free carriers investigating macroscopic areas of the samples (tens of μm^2), the technique used can be applied to samples of different size and morphology and, in combination with microphotoluminescence setups, will allow the study of single nanocrystals.

5 Conclusions

We present experimental results concerning the relaxation and thermalization process in a CsPbBr$_3$ bulk sample and microcrystal ensemble on a picosecond time scale. High resolution low temperature TR-PL measurements provide evidence of a thermalized carrier distribution, which, however, remains hotter than the lattice. Given our experimental conditions, such a relaxation bottleneck cannot be explained by the Auger effect or hot phonon population; it can tentatively be ascribed to a long-living population released by high energy traps, the origin of which is eventually related to surfaces; an additional investigation regarding this point is in progress. Moreover, significant long-lasting non-linearities in the emission are found. The measured photoinduced PL decrease comes from the saturation of the localized/bound states, whereas the photoinduced PL increase observed in the high energy side of the PL spectrum can be related to the bimolecular radiative recombination from the free carrier population.

References

[1] Xiao Z, Yuan Y, Wang Q, et al. Thin-film semiconductor perspective of organometal trihalide perovskite materials for high-efficiency solar cells. Mater Sci Eng R 2016;101:1–38.

[2] Green MA, Ho-Baillie A. Perovskite solar cells: the birth of a new era in photovoltaics. ACS Energy Lett 2017;2:822–30.

[3] Polman A, Knight M, Garnett EC, Ehrler B, Sinke WC. Photovoltaic materials: present efficiencies and future challenges. Science 2016;352:aad4424.

[4] Kim Y-H, Cho H, Lee T-W. Metal halide perovskite light emitters. PNAS 2016;113:11694–702.

[5] Veldhuis SA, Boix PP, Yantara N, et al. Perovskite materials for light-emitting diodes and lasers. Adv Mater 2016;28:6804–34.

[6] Yakunin S, Protesescu L, Krieg F, et al. Low-threshold amplified spontaneous emission and lasing from colloidal nanocrystals of caesium lead halide perovskites. Nat Commun 2015;6:8056.

[7] Li Z, Moon J, Gharajeh A, et al. Room-temperature continuous-wave operation of organometal halide perovskite lasers. ACS Nano 2018;12:10968–76.

[8] Zhuang Y, Yuan W, Qian L, Chen S, Shi G. High-performance gas sensors based on a thiocyanate ion-doped organometal halide perovskite. Phys Chem Chem Phys 2017;19:12876–81.

[9] Wang K, Li G, Wang S, et al. Dark-field sensors based on organometallic halide perovskite microlasers. Adv Mater 2018;30:e1801481.

[10] Huang J, Lai M, Lin J, Yang P. Rich chemistry in inorganic halide perovskite nanostructures. Adv Mater 2018;30:1802856.

[11] Asghar MI, Zhang J, Wang H, Lund PD. Device stability of perovskite solar cells – A review. Renewable Sustainable Energy Rev 2017;77:131–46.

[12] Salhi B, Wudil YS, Hossain MK, Al-Ahmed A, Al-Sulaiman FA. Review of recent developments and persistent challenges in stability of perovskite solar cells. Renewable Sustainable Energy Rev 2018;90:210–22.

[13] Snaith HJ, Hacke P. Enabling reliability assessments of pre-commercial perovskite photovoltaics with lessons learned from industrial standards. Nat Energy 2018;3:459–65.

[14] Protesescu L, Yakunin S, Bodnarchuk MI, et al. Nanocrystals of cesium lead halide perovskites (CsPbX3, X = Cl, Br, and I): novel optoelectronic materials showing bright emission with wide color gamut. Nano Lett 2015;15:3692–6.

[15] Stoumpos CC, Malliakas CD, Peters JA, et al. Crystal growth of the perovskite semiconductor cspbbr$_3$: a new material for high-energy radiation detection. Cryst Growth Des 2013;13:2722–7.

[16] He Y, Matei L, Jung HJ, et al. High spectral resolution of gamma-rays at room temperature by perovskite CsPbBr3 single crystals. Nat Commun 2018;9:1609.

[17] Shi D, Adinolfi V, Comin R, et al. Low trap-state density and long carrier diffusion in organolead trihalide perovskite single crystals. Science 2015;347:519–22.

[18] Ding J, Du S, Zuo Z, Zhao Y, Cui H, Zhan X. High detectivity and rapid response in perovskite CsPbBr3 single-crystal photodetector. J Phys Chem C 2017;121:4917–23.

[19] Sebastian M, Peters JA, Stoumpos CC, et al. Excitonic emissions and above-band-gap luminescence in the single-crystal perovskite semiconductors CsPbBr$_3$ and CsPbCl$_3$. Phys Rev B 2015;92:235210.

[20] Li J, Yuan X, Jing P, et al. Temperature-dependent photoluminescence of inorganic perovskite nanocrystal films. RSC Adv 2016;6:78311–6.

[21] Diroll BT, Zhou H, Schaller RD. Low-temperature absorption, photoluminescence, and lifetime of CsPbX3 (X = Cl, Br, I) nanocrystals. Adv Funct Mater 2018;28:1800945.

[22] Becker MA, Vaxenburg R, Nedelcu G, et al. Bright triplet excitons in caesium lead halide perovskites. Nature 2018;553:189–94.

[23] Yang Y, Yang M, Moore DT, et al. Top and bottom surfaces limit carrier lifetime in lead iodide perovskite films. Nat Energy 2017;2:16207.

[24] Zhang H, Liu X, Dong J, et al. Centimeter-sized inorganic lead halide perovskite CsPbBr$_3$ crystals grown by an improved solution method. Cryst Growth Des 2017;17:6426–31.

[25] Bruzzi M, Gabelloni F, Calisi N, Caporali S, Vinattieri A. Defective states in micro-crystalline CsPbBr$_3$ and their role on photoconductivity. Nanomaterials 2019;9:177.

[26] Shah J. Ultrafast spectroscopy of semiconductors and semiconductor nanostructure. Heidelberg, Springer-Verlag, 1996.

[27] Pau S, Kuhl J, Khan MA, Sun CJ. Application of femtosecond-excitation correlation to the study of emission dynamics in hexagonal GaN. Phys Rev B 1998;58:12916–9.

[28] Vinattieri A, Bogani F, Cavigli L, et al. Large-k exciton dynamics in GaN epilayers: Nonthermal and thermal regimes. Phys Rev B 2013;87:075202.

[29] Ulbrich R. Energy relaxation of photoexcited hot electrons in GaAs. Phys Rev B 1973;8:5719–27.

[30] Grote C, Berger RF. Strain tuning of tin-halide and lead-halide perovskites: a first-principles atomic and electronic structure study. J Phys Chem C 2015;119:22832–7.

[31] Yang J, Wen X, Xia H, et al. Acoustic-optical phonon up-conversion and hot-phonon bottleneck in lead-halide perovskites. Nat Commun 2017;8:14120.

[32] Zhu H, Miyata K, Fu Y, et al. Screening in crystalline liquids protects energetic carriers in hybrid perovskites. Science 2016;353:1409–13.

[33] Yang Y, Ostrowski DP, France RM, et al. Observation of a hot-phonon bottleneck in lead-iodide perovskites. Nat Photonics 2016;10:53–9.

[34] Li M, Bhaumik S, Goh TW, et al. Slow cooling and highly efficient extraction of hot carriers in colloidal perovskite nanocrystals. Nat Commun 2017;8:14350.

[35] Niesner D, Zhu H, Miyata K, et al. Persistent energetic electrons in methylammonium lead iodide perovskite thin films. J Am Chem Soc 2016;138:15717–26.

[36] Miyata K, Meggiolaro D, Trinh MT, et al. Large polarons in lead halide perovskites. Sci Adv 2017;3:e1701217.

[37] de Jong EMLD, Yamashita G, Gomez L, Ashida M, Fujiwara Y, Gregorkiewicz T. Multiexciton lifetime in all-inorganic CsPbBr$_3$ perovskite nanocrystals. J Phys Chem C 2017;121:1941–7.

[38] Liu Q, Wang Y, Sui N, et al. Exciton relaxation dynamics in photo-excited cspbi$_3$ perovskite nanocrystals. Sci Rep 2016;6:29442.

[39] Wang Y, Wang Y, Verma SD, et al. Concentration dependent carriers dynamics in CsPbBr$_3$ perovskite nanocrystals film with transient grating. Appl Phys Lett 2017;110:181910.

[40] Makarov NS, Guo S, Isaienko O, Liu W, Robel I, Klimov VI. Spectral and dynamical properties of single excitons, biexcitons, and trions in cesium–lead-halide perovskite quantum dots. Nano Lett 2016;16:2349–62.

[41] Papagiorgis P, Protesescu L, Kovalenko MV, Othonos A, Itskos G. Long-lived hot carriers in formamidinium lead iodide nanocrystals. J Phys Chem C 2017;121:12434–40.

[42] Kawai H, Giorgi G, Marini A, Yamashita K. The mechanism of slow hot-hole cooling in lead-iodide perovskite: first-principles calculation on carrier lifetime from electron–phonon interaction. Nano Lett 2015;15:3103–8.

[43] Gabelloni F, Biccari F, Andreotti G, et al. Recombination dynamics in CsPbBr$_3$ nanocrystals: role of surface states. Opt Mater Express 2017;7:4367–73.

[44] Reimand I, Aaviksoo J. Exciton interaction with hot electrons in GaAs. Phys Rev B 2000;61:16653–8.